

---

*Research Article: New Research / Development*

## **Super-Resolution Microscopy Reveals a Nanoscale Organization of Acetylcholine Receptors for Trans-Synaptic Alignment at Neuromuscular Synapses**

### **Spatial Distribution of AChRs at the NMJ**

**Amanda L. York<sup>1</sup> and James Q. Zheng<sup>1,2,3</sup>**

<sup>1</sup>*Department of Cell Biology, Emory University School of Medicine, Atlanta, GA 30322*

<sup>2</sup>*Department of Neurology, Emory University School of Medicine, Atlanta, GA 30322*

<sup>3</sup>*Center for Neurodegenerative Disease, Emory University School of Medicine, Atlanta, GA 30322*

DOI: 10.1523/ENEURO.0232-17.2017

Received: 4 July 2017

Revised: 24 July 2017

Accepted: 25 July 2017

Published: 31 July 2017

---

**Author contributions:** A.L.Y. performed all the experiments and quantitative analyses, and drafted the manuscript. A.L.Y. and J.Q.Z. designed the project and wrote the manuscript. J.Q.Z. oversaw the project.

**Funding:** HHS | NIH | National Institute of General Medical Sciences (NIGMS): 100000057; GM083889. HHS | NIH | National Institute of Mental Health (NIMH): 100000025; MH104632. HHS | NIH | National Institute of Mental Health (NIMH): 100000025; MH108025. HHS | NIH | National Institute on Aging (NIA): 100000049; AG051510. HHS | NIH | National Institute of Neurological Disorders and Stroke (NINDS): 100000065; NS082007. HHS | NIH | National Institute of Neurological Disorders and Stroke (NINDS): 100000065; NS090083. HHS | NIH | National Institute of Neurological Disorders and Stroke (NINDS): 100000065; NS055077.

The authors declare no competing or financial interests.

National Institute of General Medical Sciences (NIGMS) 100000057, GM083889; HHS | NIH | National Institute of Mental Health (NIMH) 100000025, MH104632, MH108025; HHS | NIH | National Institute on Aging (NIA) 100000049, AG051510; HHS | NIH | National Institute of Neurological Disorders and Stroke (NINDS), 100000065, NS082007; HHS | NIH | National Institute of Neurological Disorders and Stroke (NINDS), 100000065, NS090083; HHS | NIH | National Institute of Neurological Disorders and Stroke (NINDS), 100000065, NS055077.

**Correspondence:** James Q. Zheng, Department of Cell Biology, Emory University School of Medicine, 615 Michael Street, Atlanta, GA 30322. E-mail: [james.zheng@emory.edu](mailto:james.zheng@emory.edu)

**Cite as:** eNeuro 2017; 10.1523/ENEURO.0232-17.2017

**Alerts:** Sign up at [eneuro.org/alerts](http://eneuro.org/alerts) to receive customized email alerts when the fully formatted version of this article is published.

Accepted manuscripts are peer-reviewed but have not been through the copyediting, formatting, or proofreading process.

Copyright © 2017 York and Zheng

This is an open-access article distributed under the terms of the Creative Commons Attribution 4.0 International license, which permits unrestricted use, distribution and reproduction in any medium provided that the original work is properly attributed.

1 **Super-resolution microscopy reveals a nanoscale**  
2 **organization of acetylcholine receptors for trans-synaptic**  
3 **alignment at neuromuscular synapses**

4  
5 <sup>1</sup> Amanda L. York and <sup>1,2,3</sup> James Q. Zheng

6 <sup>1</sup> Department of Cell Biology, Emory University School of Medicine, Atlanta, GA 30322.

7 <sup>2</sup> Department of Neurology, <sup>3</sup> Center for Neurodegenerative Disease, Emory University  
8 School of Medicine, Atlanta, GA 30322.

9  
10  
11  
12 Abbreviated Title: Spatial Distribution of AChRs at the NMJ

13 Number of words: Abstract: 234; Introduction: 691; Discussion: 1112

14 Number of pages: 28

15 Number of figures: 5

16 Key words: neuromuscular synapse, NMJ, junctional folds, super-resolution microscopy,  
17 synaptic receptors, spatial distribution

18 Correspondence: James Q. Zheng, Department of Cell Biology, Emory University

19 School of Medicine, 615 Michael Street, Atlanta, GA 30322. E-mail:

20 james.zheng@emory.edu.

21 Conflict of Interest: The authors declare no competing or financial interests.

22 **Abstract**

23           The neuromuscular junction (NMJ) is a chemical synapse formed between  
24 motoneurons and skeletal muscle fibers. The vertebrate NMJ uses acetylcholine as  
25 the neurotransmitter and features numerous invaginations of the postsynaptic muscle  
26 membrane termed junctional folds. Acetylcholine receptors (AChRs) are believed to be  
27 concentrated on the crest of junctional folds but their spatial organization remains to be  
28 fully understood. In this study, we utilized super-resolution microscopy to examine the  
29 nanoscale organization of AChRs at NMJ. Using Structured Illumination Microscopy,  
30 we found that AChRs appear as stripes within the pretzel-shaped mouse NMJs, which  
31 however, do not correlate with the size of the crests of junctional folds. By comparing  
32 the localization of AChRs with several pre- and post-synaptic markers of distinct  
33 compartments of NMJs, we found that AChRs are not distributed evenly across the  
34 crest of junctional folds as previously thought. Instead, AChR stripes are more closely  
35 aligned with the openings of junctional folds as well as with the presynaptic active zone.  
36 Using Stochastic Optical Reconstruction Microscopy for increased resolution, we found  
37 that each AChR stripe contains an AChR-poor slit at the center that is equivalent to the  
38 size of the opening of junctional folds. Together, these findings indicate that AChRs are  
39 largely localized to the edges of crests surrounding the opening of folds to align with the  
40 presynaptic active zones. Such a nanoscale organization of AChRs potentially enables  
41 trans-synaptic alignment for effective synaptic transmission of NMJs.

42 **Significant Statement**

43 Vertebrate neuromuscular synapses are structurally unique as the postsynaptic  
44 muscle membrane forms numerous folds in the sarcolemma that are believed to play an  
45 important role in synaptic transmission. Acetylcholine receptors (AChRs) are believed  
46 to be concentrated on the crest of junctional folds, but their spatial distribution in relation  
47 to the junctional folds remain to be fully understood. In this study, we provide evidence  
48 that AChRs are not uniformly distributed across of the crest of junctional folds, but  
49 instead locally enriched at the edges, aligning with the presynaptic active zone. Such a  
50 nanoscale organization positions AChRs for effective reception of neurotransmitters  
51 released by presynaptic motor terminals during synaptic transmission.

## 52 Introduction

53 The coordinated anatomical movement of human's everyday lives depends on  
54 rapid and precise neuromuscular communication. At the heart of this process lies the  
55 neuromuscular junction (NMJ), a specialized synapse between a motor neuron and a  
56 single muscle fiber. The NMJ is a large and topographically complex synapse  
57 compared to synapses of the central nervous system (Sanes and Lichtman, 1999; Wu  
58 et al., 2010; Shi et al., 2012). As with many biological systems, the organization and  
59 structural integrity of the NMJ is critical to its function. Defects in synaptic architecture,  
60 including misalignment of the pre- and post-synaptic terminals, are a common  
61 phenotype of many neuromuscular diseases and genetic defects (Hirsch, 2007; Slater,  
62 2008; Ha and Richman, 2015), as such mapping the precise organization of synaptic  
63 components is crucial in order to fully understand NMJ function in healthy individuals.

64 The vertebrate NMJ is marked by unique structural features. Notably, the axon  
65 terminal of a motor neuron sinks into the muscle membrane, creating a characteristic  
66 depression referred to as the primary gutter. Within this gutter, are smaller  
67 invaginations of the postsynaptic membrane, termed junctional folds. The junctional  
68 folds can be further divided into the crest, representing the top of the folds closest to the  
69 presynaptic terminal, and the trough, representing the bottom part of the infolded  
70 membrane. While the exact function of the junctional folds remains to be fully  
71 determined, they likely play a critical role in neurotransmission by providing a platform  
72 for the spatial segregation of key postsynaptic molecules. For instance, acetylcholine  
73 receptors (AChRs), are present at the crest and partially down the sides of junctional  
74 folds, whereas voltage-gated sodium channels (VGSCs) are concentrated at the trough

75 (Fertuck and Salpeter, 1974; Matthews-Bellinger and Salpeter, 1983; Flucher and  
76 Daniels, 1989). Studies involving mathematically modeling of NMJ neurotransmission  
77 in the presence or absence of junctional folds have suggested that they may act to  
78 reduce the threshold necessary for action potential firing, thus making NMJ  
79 neurotransmission more efficient (Martin, 1994).

80         The alignment of neurotransmitter release sites on the presynaptic terminal with  
81 the clusters of neurotransmitter receptors on the postsynaptic membrane represents an  
82 important mechanism that ensures efficient and effective neurotransmission in the  
83 synapses of the central nervous system (Tang et al., 2016). In vertebrate NMJs, the  
84 neurotransmitter acetylcholine (ACh) is released from highly specialized sites on the  
85 presynaptic terminal called active zones (Nishimune, 2012). Readily releasable ACh  
86 vesicles are docked at the active zones by interacting with the macromolecules in the  
87 active zone material (Harlow et al., 2013). Intriguingly, electron microscopy (EM)  
88 studies have shown that presynaptic active zones are positioned apposed to the  
89 openings of junctional folds (Couteaux and Pecot-Dechavassine, 1970; Dreyer et al.,  
90 1973; Patton et al., 2001), whereas AChRs appear to be present across the fold crest  
91 and partially down the sides of the infolded membrane (Fertuck and Salpeter, 1974;  
92 Matthews-Bellinger and Salpeter, 1983). If this configuration indeed reflects the  
93 physiological organization of the NMJ, it would mean that AChRs are, in large part,  
94 misaligned from presynaptic active zones — a finding that would theoretically reduce  
95 neurotransmission efficiency. While these EM studies provided many seminal insights  
96 into the general organization of NMJ components, a detailed analysis of AChR  
97 distribution along the junctional folds has previously been precluded by the relatively

98 sparse labeling that occurs with immuno-EM, and the limited resolution of conventional  
99 light microscopy.

100 In this study, we used super-resolution microscopy to examine the nanoscale  
101 distribution of AChRs on the postsynaptic membrane. Together with specific markers  
102 for distinct compartments of the NMJ, we present evidence that AChRs are not evenly  
103 distributed across the crest of the junctional folds, as the previous model predicts.  
104 Rather, our data reveal that AChRs are concentrated at the edge of the crest, apposed  
105 to the active zone of presynaptic terminals. As a result, the individual AChR-rich stripes  
106 seen using conventional fluorescence microscopy are actually composed of AChRs  
107 from the edges of two adjacent crests, whereas the AChR-poor space actually  
108 represents the central region of the crest, rather than the region between neighboring  
109 crests. Collectively, the results from our data builds a new model whereby AChRs on  
110 the postsynaptic membrane are concentrated under presynaptic neurotransmitter  
111 release sites, allowing for effective synaptic transmission.

112 **Materials and Methods**

113 Antibodies and chemical reagents

114 The following antibodies were used in this study: rabbit anti-alpha tubulin (1:200;  
115 Abcam, ab15246), mouse anti-rapsyn (1:100; EMD Millipore, MAB2238), rat anti-  
116 Integrin  $\alpha 7$  (1:200; R&D Systems, MAB3518), mouse anti-sodium channel (1:100;  
117 Sigma, S8809), rabbit anti-piccolo (1:500; Synaptic Systems, 142 003). Alexa Fluor 488  
118 conjugated  $\alpha$ -bungarotoxin and Alexa Fluor 647 conjugated  $\alpha$ -bungarotoxin (1:1000)  
119 were purchased from Invitrogen (B13422 & B35450, respectively).

120 Whole-mount immunofluorescence

121 Wild-type C57BL/6 mice of mixed sex were sacrificed by exposure to CO<sub>2</sub>. The  
122 pretzel-shaped distribution of AChRs as well as the junctional folds are fully developed  
123 by postnatal day 21 (Slater, 1982; Singhal and Martin, 2011). Therefore, mice between  
124 4 – 8 weeks of age were used for all experiments. All procedures were carried out in  
125 accordance with National Institutes of Health guidelines for animal use and were  
126 approved by the Institutional Animal Care and Use Committee of Emory University. The  
127 transversus abdominis (TVA) muscle was dissected as previously described by Murray  
128 *et. al.* (2014). Briefly, the entire abdominal musculature was dissected from the mouse  
129 and immediately fixed for 10 minutes in 4% (v/v) paraformaldehyde (Polysciences Inc.)  
130 in phosphate-buffered saline (PBS). Following fixation, the superficial layers of muscle  
131 were removed revealing the TVA muscle situated in the deepest layer of the abdominal  
132 wall. The TVA muscle is a very thin muscle group, making it a great candidate for  
133 successful whole-mount immunostaining. After the TVA was carefully cleaned of any

134 fat or fascia, the tissue was incubated with Alexa Fluor 488 or Alexa Fluor 647  
135 conjugated  $\alpha$ -bungarotoxin for 30 minutes to label AChRs. The tissue was then  
136 permeabilized with 2% Triton X-100 (Sigma) for 30 minutes, and blocked with 4%  
137 bovine serum albumin (BSA) and 1% Triton X-100 in PBS for at least 30 minutes. The  
138 tissue was then incubated with primary antibodies diluted in blocking buffer overnight at  
139 4°C. Following extensive washing with PBS, the tissue was incubated with secondary  
140 antibodies in blocking buffer for 2 – 4 hours. Following extensive washing with PBS, the  
141 tissue was directly mounted onto a glass slide with Fluoromount-G (SouthernBiotech).  
142 All NMJs were imaged 'en face'.

143 For STORM imaging, teased muscles were labeled with Alexa Fluor 647  
144 conjugated  $\alpha$ -bungarotoxin and imaged in a photoswitchable imaging buffer containing  
145 cysteamine (MEA), glucose, glucose oxidase, and catalase, all obtained from Sigma-  
146 Aldrich (Dempsey et al., 2011). The teased muscle fibers were weighed down on a  
147 homemade glass bottom dish in order to allow for better imaging of 'en face' NMJs.

#### 148 Microscopy and image analysis

149 Laser-scanning confocal images were collected on a Nikon C1 confocal system  
150 based on the Nikon Eclipse TE300 inverted microscope (Nikon Instruments, Melville,  
151 NY) equipped with a 60 $\times$ /1.4 numerical aperture (NA) Plan Apo oil immersion objective.  
152 Three dimensional structured illumination microscopy (3D-SIM) was performed on a  
153 Nikon N-SIM Eclipse Ti-E microscope system equipped with Perfect Focus, 100 $\times$ /1.49  
154 NA oil immersion objective, and an EMCCD camera (DU-897, Andor Technology,  
155 Belfast, UK). Stochastic optical reconstruction microscopy (STORM) was performed

156 using a Nikon Ti-E TIRF inverted microscope equipped with Perfect Focus, 488 nm and  
157 647 nm lasers, and an iXon 897 EMCCD camera (Andor). Images were acquired using  
158 a 100×/1.45 N.A. Plan Apo  $\lambda$  objective. Approximately 40,000 frames were collected  
159 using total internal reflection fluorescence (TIRF) excitation. Images were reconstructed  
160 in Nikon Elements.

161 Intensity profile line scans were performed using the original data in Nikon  
162 Elements software. The lines were drawn perpendicular to AChR stripes, near the  
163 midline of the primary gutter. For piccolo staining specifically, care was taken to place  
164 lines in an area where piccolo puncta are present. A 12 pixel line width was used to  
165 average intensities at each point along the line in order to reduce signal noise. From  
166 the intensity profile line scans, the full width at half maximum of individual AChR stripes  
167 was used to quantify the width of AChR stripes. The distance between AChR stripes  
168 was quantified using profile line scans by measuring the distance between the centers  
169 of two neighboring AChR stripes. The average width of AChR stripes was then  
170 subtracted from each 'distance between' measurement to account for each half of  
171 AChR stripe in the original measurement, thus, resulting in the width of just the  
172 fluorescently poor space between AChR stripes. Maximum intensity z-projections were  
173 created using ImageJ software (National Institutes of Health, Bethesda, MD).  
174 Colocalization analysis was performed on Imaris 8.4 software (Andor) using maximum  
175 intensity z-projected images. A mask of the synaptic area was created in order to  
176 selectively analyze the degree of colocalization within the synaptic area.

177 Transmission Electron Microscopy

178 Mouse TVA muscles were fixed with 2.5% glutaraldehyde in 0.1M cacodylate  
179 buffer (pH 7.4). Samples were then washed and post-fixed with 1% osmium tetroxide in  
180 the same buffer for 1 hour. After rinsing with de-ionized water, samples were  
181 dehydrated through an ethanol series and then placed in 100% ethanol. Following  
182 dehydration, muscle samples were infiltrated with 100% ethanol and Eponate 12 resin  
183 (Ted Pella, Inc., Redding, CA) at a 1:1 ratio overnight. After additional infiltration in  
184 Eponate 12 resin, muscle samples were placed in labeled Beem capsule and  
185 polymerized in a 60°C oven. Ultrathin sections were cut at 70-80 nanometer thick on a  
186 Leica UltraCut S ultramicrotome (Leica Microsystems Inc., Buffalo Grove, IL). Grids  
187 with ultrathin sections were stained with 5% uranyl acetate and 2% lead citrate.  
188 Ultrathin sections were imaged on a JEOL JEM-1400 transmission electron microscope  
189 (JEOL Ltd., Tokyo, Japan) equipped with a Gatan US1000 CCD camera (Gatan,  
190 Pleasanton, CA).

191 Experimental design and statistic analysis

192 All the data were collected from at least three replica of independently prepared  
193 samples. Quantified data were statistically analyzed using one-way ANOVA. The data  
194 follow a normal distribution as examined by Anderson-Darling test. P-values are  
195 provided in the corresponding figure legends.

196 **Results**

197           In this study, we sought to utilize super resolution fluorescence microscopy  
198 techniques to analyze the spatial distribution of AChRs at the NMJ. The anatomy of  
199 muscle tissue can present many hurdles in achieving clean and successful whole-mount  
200 immunostaining. While AChRs can be readily labeled by fluorescently tagged  $\alpha$ -  
201 bungarotoxin (BTX), immuno-labeling of intracellular molecules is complicated by the  
202 thick fascia that encapsulates muscle fibers. This thick fascia can limit antibody  
203 penetration and generate a significant level of background fluorescence. Here we used  
204 the Transversus Abdominis (TVA) muscle, a thin and flat muscle located within the  
205 abdominal musculature, and adapted a whole-mount protocol (Murray et al., 2014) with  
206 modifications to improve antibody penetration and immuno-labeling of molecules at  
207 NMJs (Figure 1A). Consistently, AChRs are seen concentrating at the motor neuron  
208 endplate, appearing as 'pretzels' in the center area of the muscle fibers when imaged  
209 'en face' by laser scanning microscopy (Figure 1B). An increase in magnification shows  
210 that AChRs are not distributed uniformly within the 'pretzel' pattern of NMJ but the  
211 particular spatial organization is not well resolved using the conventional light  
212 microscopy. With the modified protocol, we were able to label the microtubule network  
213 in the intact muscle fibers (Figure 1B). Consistent with previously published results,  
214 microtubules form a cage-like network surrounding the postsynaptic area (Schmidt et  
215 al., 2012). Therefore, this TVA muscle preparation and modified staining protocol allow  
216 effective antibody penetration for immunolabeling of intracellular proteins in conjunction  
217 with surface AChR labeling.

218 To better resolve the AChR distribution inside the synaptic gutters, we used  
219 three-dimensional structured illumination microscopy (SIM), which increases the  
220 resolution limit by approximately two-fold compared to conventional light microscopy  
221 (Gustafsson, 2000; Gustafsson et al., 2008). Using SIM imaging we found that AChRs  
222 are distributed in a 'stripe' pattern, where highly fluorescent AChR stripes are separated  
223 by fluorescently poor space (appearing as dark bands) (Figure 2A). Since AChRs are  
224 thought to be concentrated across the crests of junctional folds and absent from the  
225 trough of junctional folds, the highly fluorescent AChR stripes could represent the crests  
226 of junctional folds separated by the AChR-poor infolded region. To examine this  
227 possibility, we performed quantitative analysis on the widths of the AChR stripes and  
228 the dark bands by generating intensity profiles (Figure 2B). Our data show that the  
229 average width of the AChR stripes is  $149 \pm 28$  nm (mean  $\pm$  standard deviation),  
230 whereas the AChR-poor bands have a width of  $188 \pm 66$  nm. To determine if these  
231 numbers represent the crests or the openings of to the junctional folds, we performed  
232 transmitted electron microscopy (TEM) on TVA muscles and quantified the average  
233 widths of the junctional fold crests and openings (Figure 2C). We found that the  
234 openings of the infoldings have a size of  $55 \pm 9$  nm, which is significantly smaller than  
235 the width of the dark bands observed with fluorescent staining (Figure 2D). Even  
236 considering the difference in resolution limits, the width of the fluorescently-poor dark  
237 bands between stripes is significantly larger and does not correlate with the opening of  
238 the membrane infoldings. However, the average distance between AChR stripes ( $188 \pm$   
239  $66$  nm) correlates with the average width of fold crests from EM data ( $207 \pm 61$  nm)

240 within the margin of error (Figure 2D). Therefore, the AChR-rich and -poor stripes are  
241 not directly related to the crests and openings to troughs, respectively.

242 To better understand the relationship between the AChR stripes and junctional  
243 folds, we sought to compare the subsynaptic distribution of AChRs to various markers  
244 with known localizations. We first compared the subsynaptic localization of AChR and  
245 rapsyn. Rapsyn is a highly characterized intracellular protein that immobilizes AChRs at  
246 the postsynaptic membrane through scaffolding connections with the underlying actin  
247 network (Walker et al., 1984; Antolik et al., 2007). Therefore, we would expect rapsyn  
248 to exhibit a very high degree of colocalization with AChRs. Indeed,  
249 immunofluorescence of AChRs and rapsyn revealed that they precisely overlap with  
250 one another (Figure 3A, top row). Intensity line profiles of these two signals greatly  
251 overlap, supporting the visual impression of colocalization (Figure 3B), which is further  
252 confirmed by the colocalization analysis (Figure 3C, Manders Coefficient =  $82.2\% \pm$   
253  $7.7\%$ ).

254 Previous EM studies have shown that active zones on the presynaptic terminal  
255 precisely align with the opening of the postsynaptic infoldings (Couteaux and Pecot-  
256 Dechavassine, 1970; Dreyer et al., 1973; Patton et al., 2001). Therefore, we used an  
257 antibody specific for the active zone protein piccolo to mark the area representing the  
258 opening of postsynaptic membrane infoldings. Previous studies have shown that  
259 immunofluorescence of active zones at mammalian NMJs appear as discrete puncta  
260 (Chen et al., 2012). Consistent with the literature, our immunostaining for piccolo  
261 revealed a punctate pattern marking the active zones of the mammalian NMJ. When  
262 analyzing the piccolo and AChR staining together, we found that the vast majority of

263 piccolo puncta are localized on top of AChR stripes (Figure 3A, second row). A  
264 representative profile line scan depicts the overlapping nature of piccolo and AChR  
265 staining (Figure 3B). Additionally, colocalization analysis reveals piccolo overlaps with  
266 AChRs to a high degree (Manders Coefficient =  $67.3\% \pm 5.4\%$ ) (Figure 3C). These  
267 data suggest that AChR stripes may be localized to the area surrounding the infolded  
268 membrane region. We also compared the localization of AChRs relative to the trough of  
269 junctional folds. Here, we double labeled AChRs and voltage-gated sodium channels  
270 (VGSCs), which have been shown to be spatially restricted to the trough of junctional  
271 folds (Flucher and Daniels, 1989). VGSC staining was found to largely overlap with  
272 AChR stripes (Manders Coefficient =  $69.4\% \pm 8.1\%$ ) (Figure 3A & 3C), which is further  
273 confirmed by the profile line scan (Figure 3B). These data, in conjunction with piccolo  
274 data, supports the hypothesis that AChRs may be spatially restricted to the area  
275 immediately surrounding the opening of infolded membrane.

276 To further test this hypothesis, we compared the localization of AChRs relative to  
277 the junctional fold crests. Integrin  $\alpha 7$  is a muscle specific transmembrane receptor that  
278 links the cell to the surrounding extracellular matrix (Song et al., 1992; Song et al.,  
279 1993). In the mature NMJ, integrin  $\alpha 7$  is restricted to the crest of junctional folds (Martin  
280 et al., 1996; Schwander et al., 2004). Therefore, we labeled integrin  $\alpha 7$  to mark the  
281 junctional fold crest and compared this staining to that of AChRs. Similar to AChRs,  
282 integrin  $\alpha 7$  also exhibits a similar 'stripe' staining pattern (Figure 3A). However, when  
283 overlaid with AChR staining it is apparent that integrin  $\alpha 7$  and AChRs occupy distinct  
284 domains from one another. Profile line scans depict the alternating pattern of AChR  
285 and integrin  $\alpha 7$  staining, where integrin  $\alpha 7$  is primarily present in the space between

286 AChR stripes (Figure 3B). Additionally, integrin  $\alpha 7$  was found to colocalize with AChRs  
287 to a much lower degree (Manders Coefficient =  $36.6\% \pm 14.6\%$ ) than that of piccolo and  
288 VSVGs (Figure 3C), suggesting that integrin and AChRs are distributed into distinct  
289 nanoscale domains. It should be noted that teased muscle fibers did not have the  
290 exactly same orientation for “en face” imaging of NMJs. As a result, a small tilt in the  
291 angle of the muscle fiber orientation could affect colocalization analysis due to the three  
292 dimensional nature of the sample. We believe that this is one of the contributing factors  
293 to the “imperfect” colocalization results observed here. Nevertheless, these findings  
294 suggest that AChRs and integrin  $\alpha 7$  occupy different domains within the junctional folds.  
295 Taken together, these data suggest that the localization of AChRs may be restricted to  
296 the area immediately surrounding the infolded region and thus absent from the center  
297 most part of the fold crest.

298         Based on previous studies and our results thus far, we hypothesize that AChRs  
299 are concentrated at the edge of junctional fold crests and part way down the sides of the  
300 infolded membrane. Since the opening of infoldings is below the resolution limit of  
301 conventional fluorescence microscopy and SIM, the fluorescent signals from two edges  
302 of neighboring crests may combine to give the appearance of a single AChR stripe. To  
303 test our hypothesis, we utilized Stochastic Optical Reconstruction Microscopy  
304 (STORM), which has a theoretical resolution limit of approximately 10 – 20 nm in the  
305 XY-axis and 50 nm in the Z-axis (Rust et al., 2006), providing us with the resolution  
306 necessary to visualize the opening of junctional folds. Similar to our SIM data, AChR  
307 staining appears as stripes within the overall ‘pretzel’ pattern of the NMJ (Figure 4A).  
308 Additionally, the size and distance between AChR stripes is consistent with our previous

309 SIM data at approximately 130 nm and 210 nm, respectively. Upon closer analysis of  
310 the AChR stripes, we observed a thin, fluorescently poor slit that runs down the center  
311 of each stripe (Figure 4B, arrows). This slit at the center of AChR stripes is clearly  
312 highlighted in a profile line scan of a representative stripe showing the decrease in  
313 AChR fluorescence at the center of the AChR stripe (Figure 4C). On average, the width  
314 of the slit is  $47 \pm 5.7$  nm (Figure 4D), which is approximately equivalent to the average  
315 width of the openings of infoldings from our EM data ( $55 \pm 8.5$  nm). Therefore, the slit  
316 running down the center of each AChR stripe likely represents the opening of the  
317 infolding of the postsynaptic membrane. This is the first evidence visualizing the  
318 opening of membrane infoldings using fluorescence microscopy. Overall, these data  
319 support the hypothesis that AChRs are concentrated at the edge of the junctional fold  
320 crests, surrounding the opening of membrane infoldings.

321 **Discussion**

322 AChRs are highly concentrated on the postsynaptic membrane of the NMJ for  
323 effective neurotransmission during muscle contraction. The large NMJs in vertebrates  
324 are structurally unique, as the postsynaptic muscle membrane forms numerous folds in  
325 the sarcolemma that are believed to play an important role in synaptic transmission  
326 (Martin, 1994; Shi et al., 2012). Not only do the junctional folds effectively increase the  
327 postsynaptic surface area, but they also provide a platform for the spatial segregation of  
328 molecules involved in distinct signaling pathways of NMJ neurotransmission. For  
329 example, AChRs are concentrated at the fold crest, whereas VGSCs are localized to  
330 the troughs of junctional folds (Flucher and Daniels, 1989). The topography of the folds  
331 and the spatial segregation of key postsynaptic proteins within them act to facilitate the  
332 amplification of synaptic current (Martin, 1994), thus allowing for more efficient  
333 neurotransmission. Previous studies using EM and light microscopy have shown that  
334 AChRs are distributed along the crest and part way down the junctional folds, but  
335 excluded from the trough (Fertuck and Salpeter, 1974; Burden et al., 1979; Matthews-  
336 Bellinger and Salpeter, 1983; Flucher and Daniels, 1989; Marques et al., 2000). While  
337 such a distribution of AChRs would position them close to the presynaptic membrane, it  
338 would not provide the best configuration for synaptic transmission given that the  
339 presynaptic active zones are not aligned with the center of the crest, but rather with the  
340 opening of membrane infoldings (Couteaux and Pecot-Dechavassine, 1970; Dreyer et  
341 al., 1973). Unfortunately, conventional light microscopy lacks the resolution to resolve  
342 nanoscale details of AChR distribution. While EM has the nanoscale resolution,  
343 immunogold labeling tends to be sparse and biochemical reaction products of

344 horseradish peroxidase may not be spatially confined. In this study, we present  
345 evidence, using two different types of super-resolution fluorescence imaging, that  
346 AChRs are concentrated at the edges of the crests of junctional folds. In this case,  
347 fluorescence from the two edges of adjacent crests comprises a single AChR stripe  
348 observed by conventional light microscopy, whereas the fluorescently poor space (the  
349 dark band) between AChR stripes actually represents the top of the fold crest. It should  
350 be noted that our data are presented as maximum intensity projections, thus the results  
351 are unlikely affected by the summation of signals on the wall of the folds. However, the  
352 Z-axis resolution is known to be limited, thus we cannot rule out the possibility that 'en  
353 face' imaging might not fully resolve AChR distribution on the wall of junctional folds.  
354 Nonetheless, the concentration of AChRs at the edges of the crests essentially creates  
355 a trans-synaptic alignment of AChRs with the presynaptic active zones where the  
356 neurotransmitter ACh is released (Figure 5). Concentrating AChRs at the crest edge  
357 would likely provide more efficient delivery of ACh to AChRs, and thus more efficient  
358 neurotransmission, rather than evenly distributing AChRs across the fold crest. A  
359 similar trans-synaptic alignment of active zones and neurotransmitter receptors has also  
360 been reported in synapses within the central nervous system (Tang et al., 2016),  
361 suggesting this trans-synaptic alignment may represent a conserved mechanism for  
362 efficient neurotransmission across various synapses.

363       Strong synaptic adhesion is important to maintain the integrity of the synapse.  
364 One of the key synaptic adhesion molecules at the NMJ is integrin  $\alpha 7$ , which associates  
365 with integrin  $\beta 1$  to form integrin  $\alpha 7\beta 1$  (Mayer, 2003; Singhal and Martin, 2011). Integrin  
366  $\alpha 7\beta 1$  binding of laminin  $\alpha 4$  at NMJs is crucial for the positioning of active zones, such

367 that the loss of laminin  $\alpha 4$  results in the misalignment of active zones with junctional  
368 folds (Patton et al., 2001; Sanes, 2003). Our data show that integrin  $\alpha 7$  and AChRs  
369 appear to occupy largely discrete domains, even though both are localized at the crest  
370 of junctional folds. The localization of integrin  $\alpha 7 \beta 1$  to the center most part of the fold  
371 crest could represent a specialized area for synaptic adhesion. It is possible that  
372 localizing integrin molecules into distinct nanodomains could enable stronger synaptic  
373 adhesion because adhesion molecules would not be interspersed with various other  
374 postsynaptic molecules. Additionally, a dense patch of adhesion molecules interacting  
375 with the presynaptic terminal through binding to the synaptic basal lamina could also act  
376 as a 'barrier', restricting the diffusion of ACh to the area of fold openings where AChRs  
377 are concentrated. Clearly, future research is needed to evaluate these possibilities.

378         The exact function of the junctional folds remains unclear. Many studies have  
379 found mutations that result in the loss of junctional folds (Noakes et al., 1995; Barik et  
380 al., 2014). However, these mutations usually result in disruptions to various other parts  
381 of the postsynaptic compartment, including AChR expression, making the study of  
382 junctional fold function very difficult. Nonetheless, studies using mathematical modeling  
383 of the NMJ have provided insight into the function of junctional folds. Modeling of  
384 neurotransmission with and without junctional folds has suggested that the folds act to  
385 amplify synaptic current following ACh release (Martin, 1994). Specifically, the amount  
386 of ACh quanta required to initiate muscle contraction is approximately double in the  
387 absence of junctional folds (Martin, 1994). Thus, in the presence of junctional folds,  
388 fewer AChRs need to be activated in order to initiate muscle contraction. Furthermore,  
389 densely clustering AChRs directly opposite that of neurotransmitter release sites could

390 provide another mechanism to further increase the efficacy of NMJ neurotransmission.  
391 Currently, there are no experimental manipulations available that can alter AChR  
392 distribution without affecting NMJ structure. However, it is exciting to speculate that  
393 tools may be developed in the future allowing detailed analysis of neurotransmission  
394 with AChRs concentrated at the edge of the infoldings vs. AChRs distributed across the  
395 fold crest.

396         Defects in junctional folds are a common phenotype of many diseases affecting  
397 the NMJ (Hirsch, 2007; Ha and Richman, 2015). For example, patients with myasthenia  
398 gravis produce antibodies targeting key postsynaptic molecules, of which AChRs are  
399 most often targeted (Hirsch, 2007; Spillane et al., 2010; Ha and Richman, 2015).  
400 Binding of the autoimmune antibodies results in the internalization of AChRs, reducing  
401 their concentration to about one-third that of normal NMJs (Lindstrom, 2000). AChR–  
402 antibody binding also results in damage to the postsynaptic membrane, which typically  
403 has reduced folds and a widened synaptic cleft (Hirsch, 2007). Consequently, patients  
404 exhibit severe muscle weakness due to a significant disruption in neurotransmission.  
405 Therefore, proper muscle function appears to be intricately linked to the structure of the  
406 postsynaptic terminal and the localization of AChRs.

407         In summary, our super-resolution imaging has revealed a distinct nanoscale  
408 pattern of AChRs on the postsynaptic membrane of NMJs. A similar nanoscale  
409 organization has also been shown in synapses of the central nervous system (Tang et  
410 al., 2016), suggesting that nanoscale organization and alignment of presynaptic and  
411 postsynaptic components may represent a conserved mechanism to ensure effective  
412 synaptic transmission.

413 **Acknowledgements**

414           This research project was supported in part by research grants from National  
415 Institutes of Health to JQZ (GM083889, MH104632, and MH108025), the Emory  
416 University Integrated Cellular Imaging Microscopy Core of the Emory Neuroscience  
417 NINDS Core Facilities grant (5P30NS055077), and the Robert P. Apkarian Integrated  
418 Electron Microscopy Core (UL1TR000454). We thank Dr. Lin Mei (Medical College of  
419 Georgia, Augusta University) for providing the initial training of NMJ preparation and  
420 labeling, as well as constructive input towards the project.

421 **Author contributions**

422           ALY performed all the experiments and quantitative analyses, and drafted the  
423 manuscript. ALY and JQZ designed the project and wrote the manuscript. JQZ  
424 oversaw the project.

425 **FIGURE LEGENDS**

426 **Figure 1.** Whole-mount immunostaining of the Transversus Abdominis (TVA) muscle for  
427 reliable detection of antigens at the NMJ. **(A)** The flow chart depicting the protocol used  
428 for clean and reliable immunostaining of muscle fibers. **(B)** Example images of the  
429 immunostaining. Top Left: A low magnification image shows NMJ innervation patterns  
430 along the TVA muscles. Integrin alpha7 (white), used to highlight the membrane of  
431 individual muscle fibers, was co-labeled with AChRs (green) to highlight the innervation  
432 pattern along the TVA muscle. Scale bar: 100  $\mu\text{m}$ . Top Right: A high magnification  
433 image of an individual NMJ shows the pretzel-shaped AChR distribution at the NMJ of a  
434 TVA muscle. Note that AChRs are not uniformly distributed. Scale bar: 5  $\mu\text{m}$ . Bottom:  
435 AChRs (green) were co-labeled with tubulin (white), an intracellular antigen, to show  
436 that the whole-mount method enables excellent antibody penetration to label the  
437 microtubule network inside the skeletal muscle. Scale bar: 20  $\mu\text{m}$ .

438 **Figure 2.** AChRs are distributed in stripes that are not correlated with the crest of NMJ  
439 junctional folds. **(A)** A representative 3D-SIM image showing the AChR-rich stripes  
440 separated by dark bands. Scale bar: 5  $\mu\text{m}$ . The areas enclosed by dashed line  
441 rectangles (A' and A'') are shown in a high magnification on the right. Scale bar: 1  $\mu\text{m}$ .  
442 **(B)** A small region of the AChR stripes (left panel) are used to generate the intensity  
443 profile shown on the right. The width of the AChR stripes (W) and the distance between  
444 two adjacent stripes (D) are measured and presented in the bar graph in **(D)**. **(C)** A  
445 representative transmission electron micrograph of an NMJ from the transversus  
446 abdominis muscle. The junctional folds are clearly visible at the postsynaptic  
447 compartment (highlighted by red color). Numerous synaptic vesicles and mitochondria

448 are present within the opposing presynaptic terminal. The average width of junctional  
449 fold openings and fold crests (red brackets) were manually quantified and presented in  
450 the bar graph in (D). Scale bar, 0.2  $\mu\text{m}$ . (D) The bar graph summarizing the  
451 measurement results from the SIM data (blue bars,  $n=4$ , >180 stripes) and EM data (red  
452 bars;  $n=7$ , >40 folds). Error bars represent the standard deviation.

453 **Figure 3.** Correlation of AChR distribution with specific pre- and post-synaptic markers  
454 at NMJs. (A-B) Colocalization of AChRs (white) with various synaptic markers  
455 (magenta, threshold). Representative fluorescent images are shown on the right and the  
456 schematics on the right depict the known localization of each synaptic marker (magenta  
457 line) with respect to the junctional folds. Scale bars: 5  $\mu\text{m}$ . The representative intensity  
458 profiles of AChRs (grey) and each of the synaptic markers (magenta) are shown in (B).  
459 Four markers were examined: Rapsyn, an intracellular AChR scaffolding protein;  
460 Piccolo, an active zone component; VGSC, voltage-gated sodium channel; integrin  $\alpha 7$ ,  
461 an integrin subunit involved in adhesion in NMJs. (C) Quantification of the  
462 colocalization of each marker with AChRs. One-way ANOVA analysis:  $p = 2.22 \times 10^{-5}$  ( $n$   
463 = 4). Error bars represent the standard deviation. Bonferroni analysis:  $*p = 0.012$ ,  $***p <$   
464 0.004.

465 **Figure 4.** Super-resolution imaging reveals AChRs are concentrated around the  
466 opening of junctional folds. (A) 3D Stochastic Optical Reconstruction Microscopy (3D-  
467 STORM) imaging of AChRs highlights the high three-dimensional nature of the  
468 postsynaptic membrane. The widths of AChR stripes (approx. 130 nm) and the distance  
469 between stripes (approx. 210 nm) is consistent with quantifications from our previous  
470 SIM data. A small region outlined by dashed rectangle (A') is shown in a higher

471 magnification on the right. Color scale bar indicates Z-depth. Scale bars: 2  $\mu\text{m}$ . **(B)**  
472 Representative STORM images of AChRs in a NMJ. Scale bar: 5  $\mu\text{m}$ . Inset image  
473 shows the same NMJ imaged using widefield microscopy. Close-up regions (B' & B'')  
474 reveals a thin slit at the center of each AChR stripe (arrow). Scale bar: 1  $\mu\text{m}$ . Bottom,  
475 close-up view of individual AChR stripes. **(C)** Representative profile linescan further  
476 highlighting the slit at the center of each AChR stripe. **(D)** Quantification of the width of  
477 the AChR stripe gap (measured from STORM data,  $n = 23$ ) and the width of the  
478 junctional fold opening (measured from our TEM data,  $n = 50$ ). Error bars represent the  
479 standard deviation. Average width values at center of each bar.

480 **Figure 5.** Schematics showing the current view **(A)** and the proposed revision **(B)** of  
481 AChR distribution along junctional fold crests. Classically, it is believed that AChRs (red)  
482 are distributed across the entire junctional fold crest and partially down the sides of the  
483 infolded membrane and excluded from the trough of junctional folds where voltage-  
484 gated sodium channels (VGSC, green) are localized **(A)**. However, we propose that  
485 AChRs are instead spatially restricted to the area immediately surrounding the opening  
486 of junctional folds and are segregated from the adhesion molecule integrin  $\alpha 7\beta 1$  (tan)  
487 located at the center-most part of fold crests **(B)**. The spatial segregation of AChRs and  
488 integrin  $\alpha 7\beta 1$  could be beneficial to maintaining strong synaptic adhesion between the  
489 pre- and postsynaptic terminals. Furthermore, this subsynaptic organization would  
490 position AChRs directly opposite that of the active zone (AZ, blue bracket), and thus, in  
491 the prime position to receive and respond to acetylcholine (dots) release.

492 **REFERENCES**

- 493 Antolik C, Catino DH, O'Neill AM, Resneck WG, Ursitti JA, Bloch RJ (2007) The actin  
494 binding domain of ACF7 binds directly to the tetratricopeptide repeat domains of  
495 rapsyn. *Neuroscience* 145:56-65.
- 496 Barik A, Lu Y, Sathyamurthy A, Bowman A, Shen C, Li L, Xiong WC, Mei L (2014) LRP4  
497 is critical for neuromuscular junction maintenance. *J Neurosci* 34:13892-13905.
- 498 Burden SJ, Sargent PB, McMahan UJ (1979) Acetylcholine receptors in regenerating  
499 muscle accumulate at original synaptic sites in the absence of the nerve. *J Cell*  
500 *Biol* 82:412-425.
- 501 Chen J, Mizushige T, Nishimune H (2012) Active zone density is conserved during  
502 synaptic growth but impaired in aged mice. *J Comp Neurol* 520:434-452.
- 503 Couteaux R, Pecot-Dechavassine M (1970) [Synaptic vesicles and pouches at the level  
504 of "active zones" of the neuromuscular junction]. *C R Acad Sci Hebd Seances*  
505 *Acad Sci D* 271:2346-2349.
- 506 Dempsey GT, Vaughan JC, Chen KH, Bates M, Zhuang X (2011) Evaluation of  
507 fluorophores for optimal performance in localization-based super-resolution  
508 imaging. *Nat Methods* 8:1027-1036.
- 509 Dreyer F, Peper K, Akert K, Sandri C, Moor H (1973) Ultrastructure of the "active zone"  
510 in the frog neuromuscular junction. *Brain Res* 62:373-380.
- 511 Fertuck HC, Salpeter MM (1974) Localization of acetylcholine receptor by 125I-labeled  
512 alpha-bungarotoxin binding at mouse motor endplates. *Proc Natl Acad Sci U S A*  
513 71:1376-1378.
- 514 Flucher BE, Daniels MP (1989) Distribution of Na<sup>+</sup> channels and ankyrin in  
515 neuromuscular junctions is complementary to that of acetylcholine receptors and  
516 the 43 kd protein. *Neuron* 3:163-175.
- 517 Gustafsson MG (2000) Surpassing the lateral resolution limit by a factor of two using  
518 structured illumination microscopy. *J Microsc* 198:82-87.

- 519 Gustafsson MG, Shao L, Carlton PM, Wang CJ, Golubovskaya IN, Cande WZ, Agard  
520 DA, Sedat JW (2008) Three-dimensional resolution doubling in wide-field  
521 fluorescence microscopy by structured illumination. *Biophys J* 94:4957-4970.
- 522 Ha JC, Richman DP (2015) Myasthenia gravis and related disorders: Pathology and  
523 molecular pathogenesis. *Biochim Biophys Acta* 1852:651-657.
- 524 Harlow ML, Szule JA, Xu J, Jung JH, Marshall RM, McMahan UJ (2013) Alignment of  
525 synaptic vesicle macromolecules with the macromolecules in active zone  
526 material that direct vesicle docking. *PLoS one* 8:e69410.
- 527 Hirsch NP (2007) Neuromuscular junction in health and disease. *Br J Anaesth* 99:132-  
528 138.
- 529 Lindstrom JM (2000) Acetylcholine receptors and myasthenia. *Muscle Nerve* 23:453-  
530 477.
- 531 Marques MJ, Conchello JA, Lichtman JW (2000) From plaque to pretzel: fold formation  
532 and acetylcholine receptor loss at the developing neuromuscular junction. *J*  
533 *Neurosci* 20:3663-3675.
- 534 Martin AR (1994) Amplification of neuromuscular transmission by postjunctional folds.  
535 *Proc Biol Sci* 258:321-326.
- 536 Martin PT, Kaufman SJ, Kramer RH, Sanes JR (1996) Synaptic integrins in developing,  
537 adult, and mutant muscle: selective association of alpha1, alpha7A, and alpha7B  
538 integrins with the neuromuscular junction. *Dev Biol* 174:125-139.
- 539 Matthews-Bellinger JA, Salpeter MM (1983) Fine structural distribution of acetylcholine  
540 receptors at developing mouse neuromuscular junctions. *J Neurosci* 3:644-657.
- 541 Mayer U (2003) Integrins: redundant or important players in skeletal muscle? *J Biol*  
542 *Chem* 278:14587-14590.
- 543 Murray L, Gillingwater TH, Kothary R (2014) Dissection of the transversus abdominis  
544 muscle for whole-mount neuromuscular junction analysis. *J Vis Exp*:e51162.

- 545 Nishimune H (2012) Active zones of mammalian neuromuscular junctions: formation,  
546 density, and aging. *Ann N Y Acad Sci* 1274:24-32.
- 547 Noakes PG, Gautam M, Mudd J, Sanes JR, Merlie JP (1995) Aberrant differentiation of  
548 neuromuscular junctions in mice lacking s-laminin/laminin beta 2. *Nature*  
549 374:258-262.
- 550 Patton BL, Cunningham JM, Thyboll J, Kortessmaa J, Westerblad H, Edstrom L,  
551 Tryggvason K, Sanes JR (2001) Properly formed but improperly localized  
552 synaptic specializations in the absence of laminin alpha4. *Nat Neurosci* 4:597-  
553 604.
- 554 Rust MJ, Bates M, Zhuang X (2006) Sub-diffraction-limit imaging by stochastic optical  
555 reconstruction microscopy (STORM). *Nat Methods* 3:793-795.
- 556 Sanes JR (2003) The basement membrane/basal lamina of skeletal muscle. *J Biol*  
557 *Chem* 278:12601-12604.
- 558 Sanes JR, Lichtman JW (1999) Development of the vertebrate neuromuscular junction.  
559 *Annu Rev Neurosci* 22:389-442.
- 560 Schmidt N, Basu S, Sladeczek S, Gatti S, van Haren J, Treves S, Pielage J, Galjart N,  
561 Brenner HR (2012) Agrin regulates CLASP2-mediated capture of microtubules at  
562 the neuromuscular junction synaptic membrane. *J Cell Biol* 198:421-437.
- 563 Schwander M, Shirasaki R, Pfaff SL, Muller U (2004) Beta1 integrins in muscle, but not  
564 in motor neurons, are required for skeletal muscle innervation. *J Neurosci*  
565 24:8181-8191.
- 566 Shi L, Fu AK, Ip NY (2012) Molecular mechanisms underlying maturation and  
567 maintenance of the vertebrate neuromuscular junction. *Trends Neurosci* 35:441-  
568 453.
- 569 Singhal N, Martin PT (2011) Role of extracellular matrix proteins and their receptors in  
570 the development of the vertebrate neuromuscular junction. *Dev Neurobiol*  
571 71:982-1005.
- 572 Slater CR (1982) Postnatal maturation of nerve-muscle junctions in hindlimb muscles of  
573 the mouse. *Dev Biol* 94:11-22.

- 574 Slater CR (2008) Structural factors influencing the efficacy of neuromuscular  
575 transmission. *Ann N Y Acad Sci* 1132:1-12.
- 576 Song WK, Wang W, Foster RF, Bielser DA, Kaufman SJ (1992) H36-alpha 7 is a novel  
577 integrin alpha chain that is developmentally regulated during skeletal  
578 myogenesis. *J Cell Biol* 117:643-657.
- 579 Song WK, Wang W, Sato H, Bielser DA, Kaufman SJ (1993) Expression of alpha 7  
580 integrin cytoplasmic domains during skeletal muscle development: alternate  
581 forms, conformational change, and homologies with serine/threonine kinases and  
582 tyrosine phosphatases. *J Cell Sci* 106 ( Pt 4):1139-1152.
- 583 Spillane J, Beeson DJ, Kullmann DM (2010) Myasthenia and related disorders of the  
584 neuromuscular junction. *J Neurol Neurosurg Psychiatry* 81:850-857.
- 585 Tang AH, Chen H, Li TP, Metzbower SR, MacGillavry HD, Blanpied TA (2016) A trans-  
586 synaptic nanocolumn aligns neurotransmitter release to receptors. *Nature*  
587 536:210-214.
- 588 Walker JH, Boustead CM, Witzemann V (1984) The 43-K protein, v1, associated with  
589 acetylcholine receptor containing membrane fragments is an actin-binding  
590 protein. *EMBO J* 3:2287-2290.
- 591 Wu H, Xiong WC, Mei L (2010) To build a synapse: signaling pathways in  
592 neuromuscular junction assembly. *Development* 137:1017-1033.
- 593

A

**DISSECTION**

- Mouse thin TVA muscles



**FIXATION**

- 4% PFA in PBS for 10 min



**AChR labeling**

- Fluorescent  $\alpha$ -BTX for 30 min



**PERMEABILIZATION**

- 2% Triton X-100 for 30 min



**BLOCKING**

- 4% BSA + 1% Triton X-100 in PBS for 30 min



**Immunostaining**

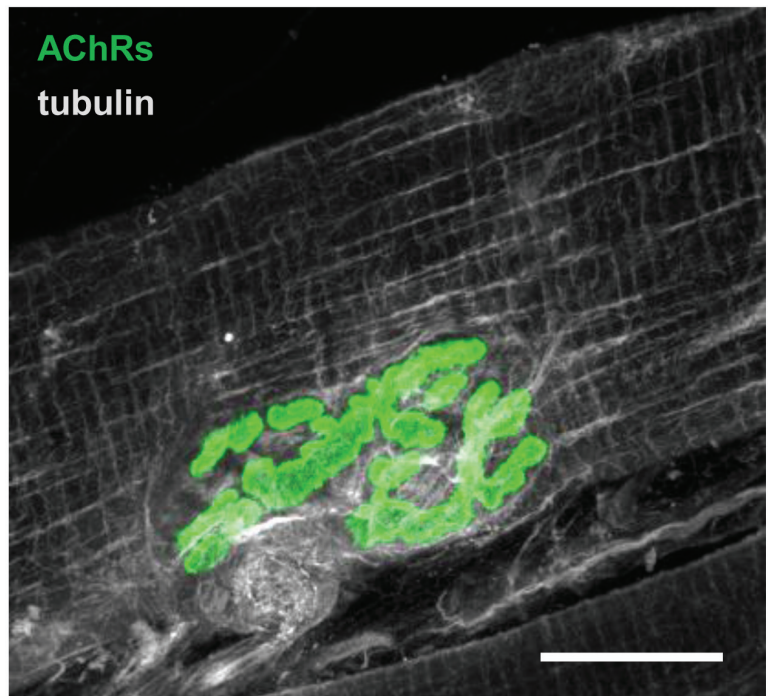
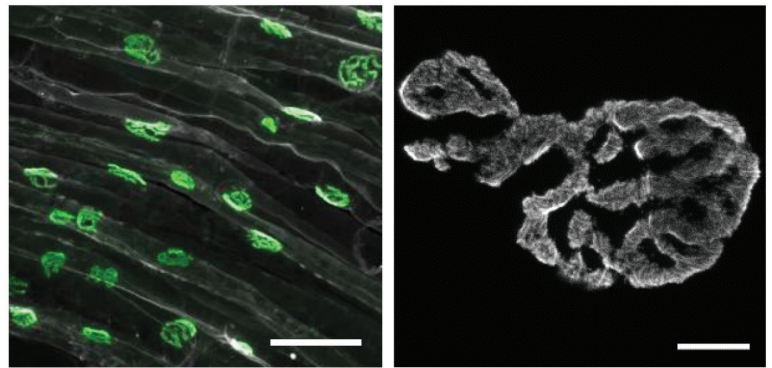
- Primary antibodies at 4 °C overnight
- Secondary antibodies at room temperature for 2-4 hr

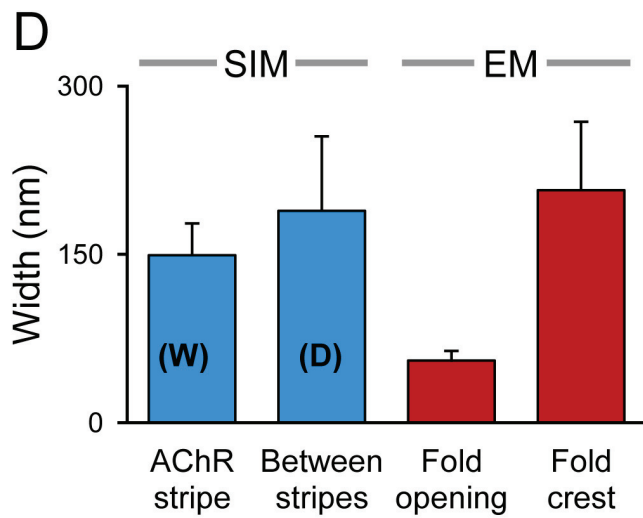
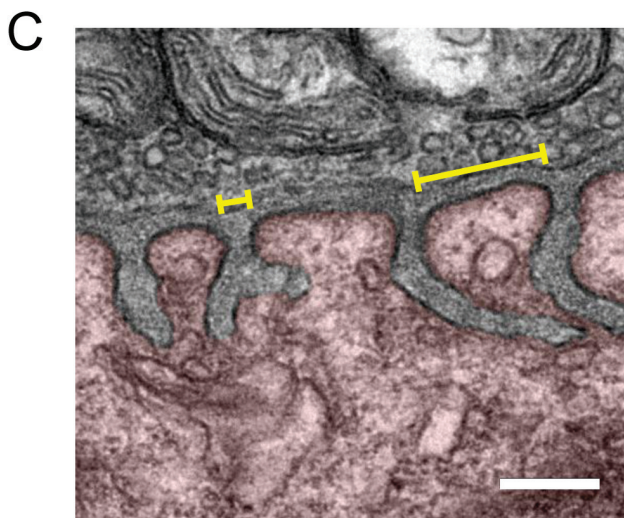
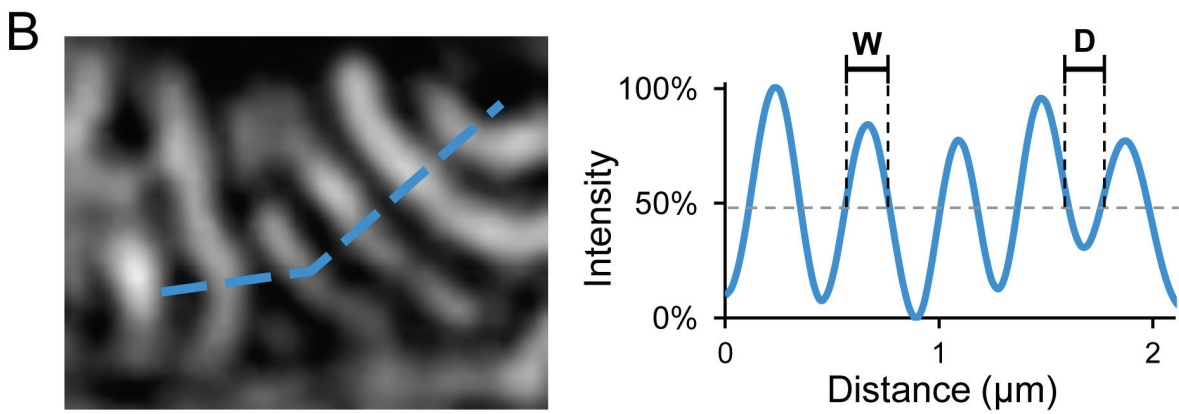
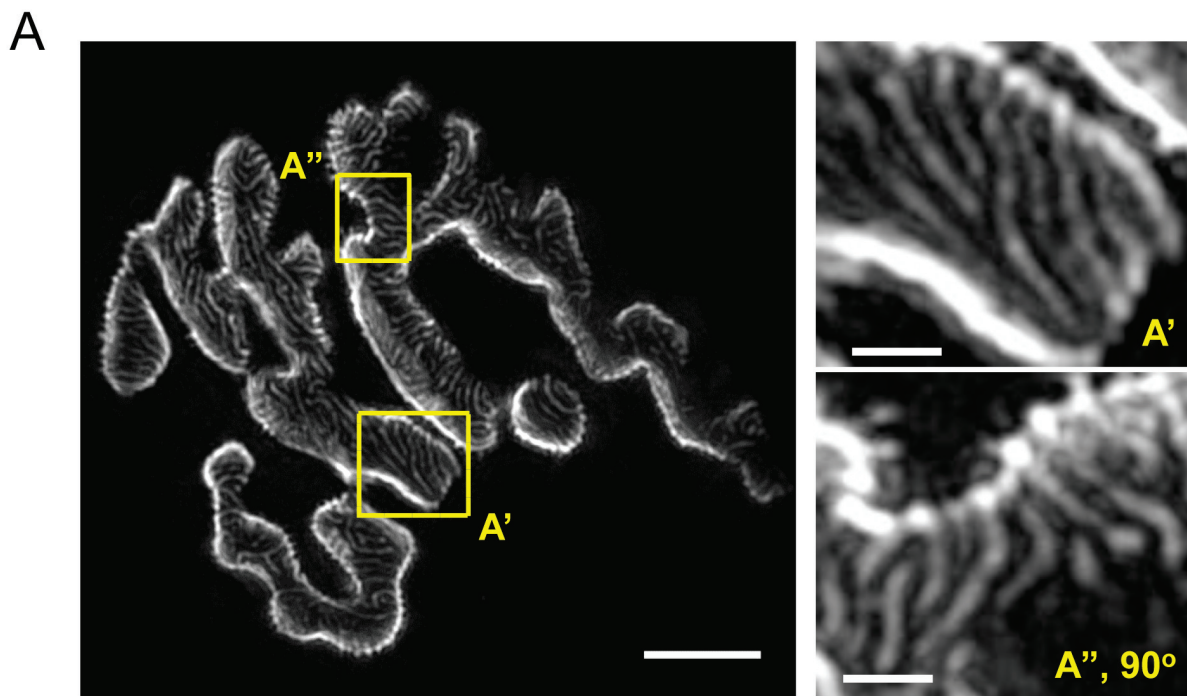


**MOUNT**

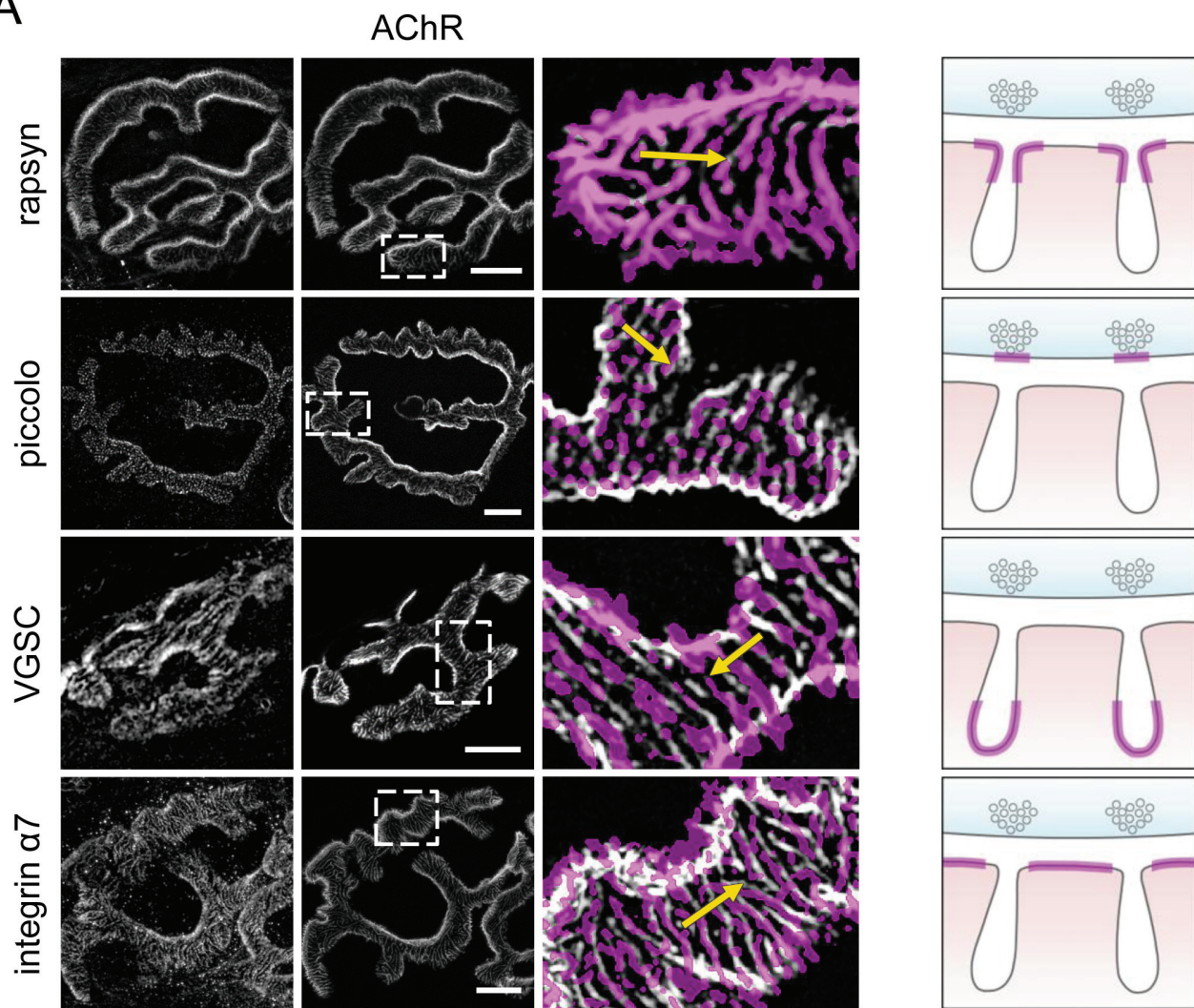
- On glass slide with mounting media & No. 1.5 coverslip

B

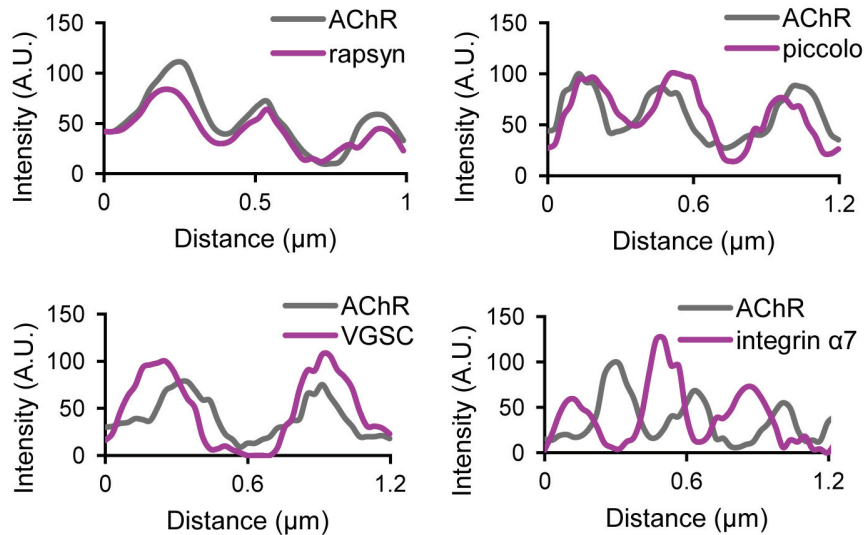




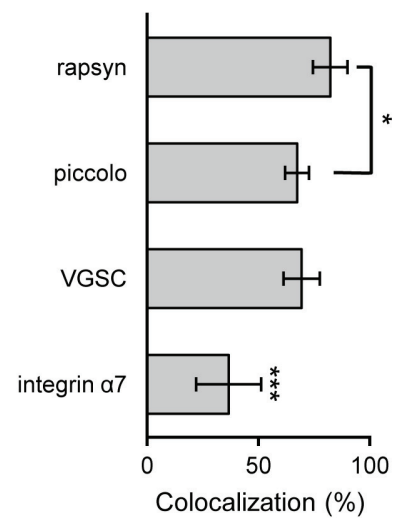
A

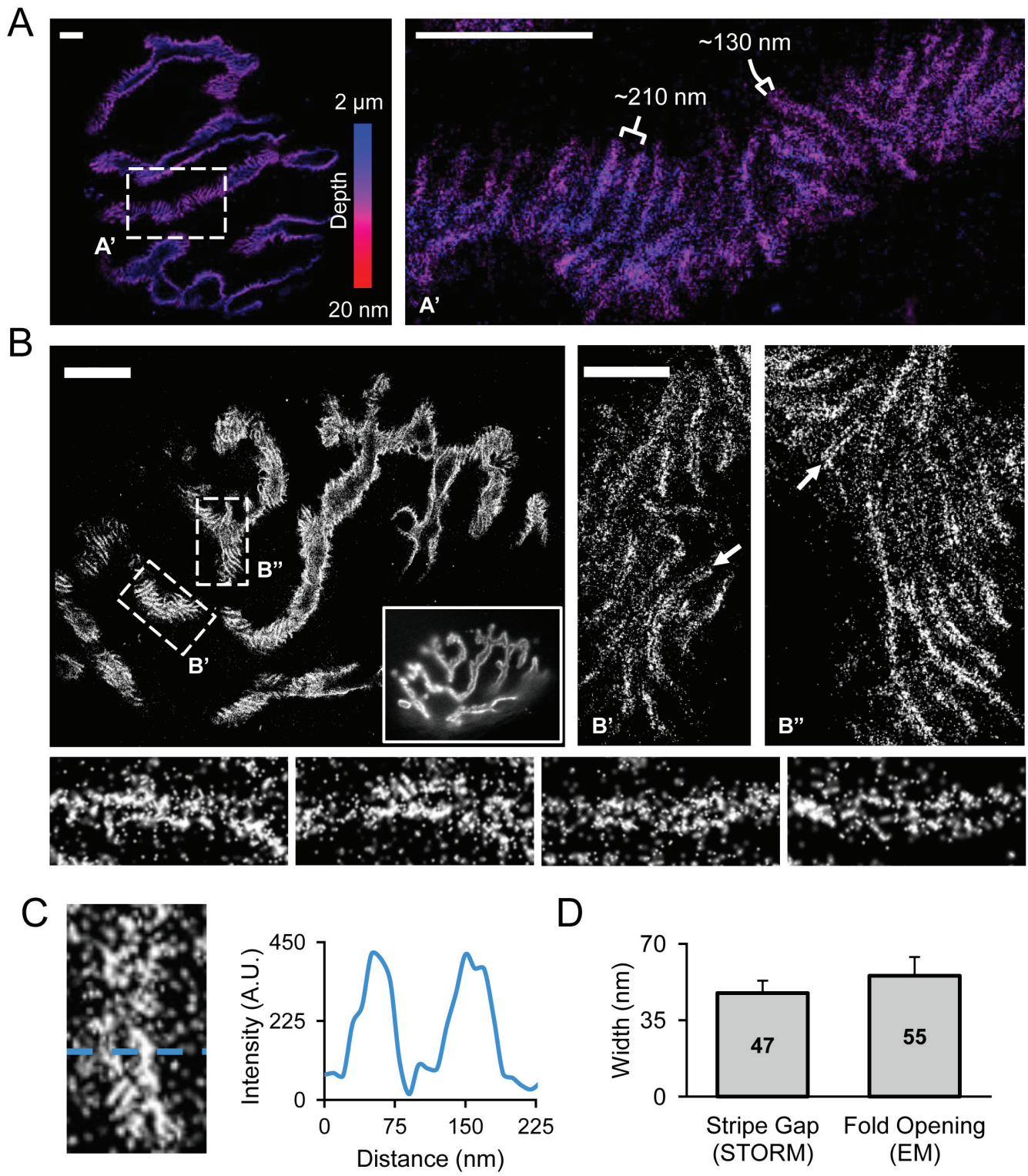


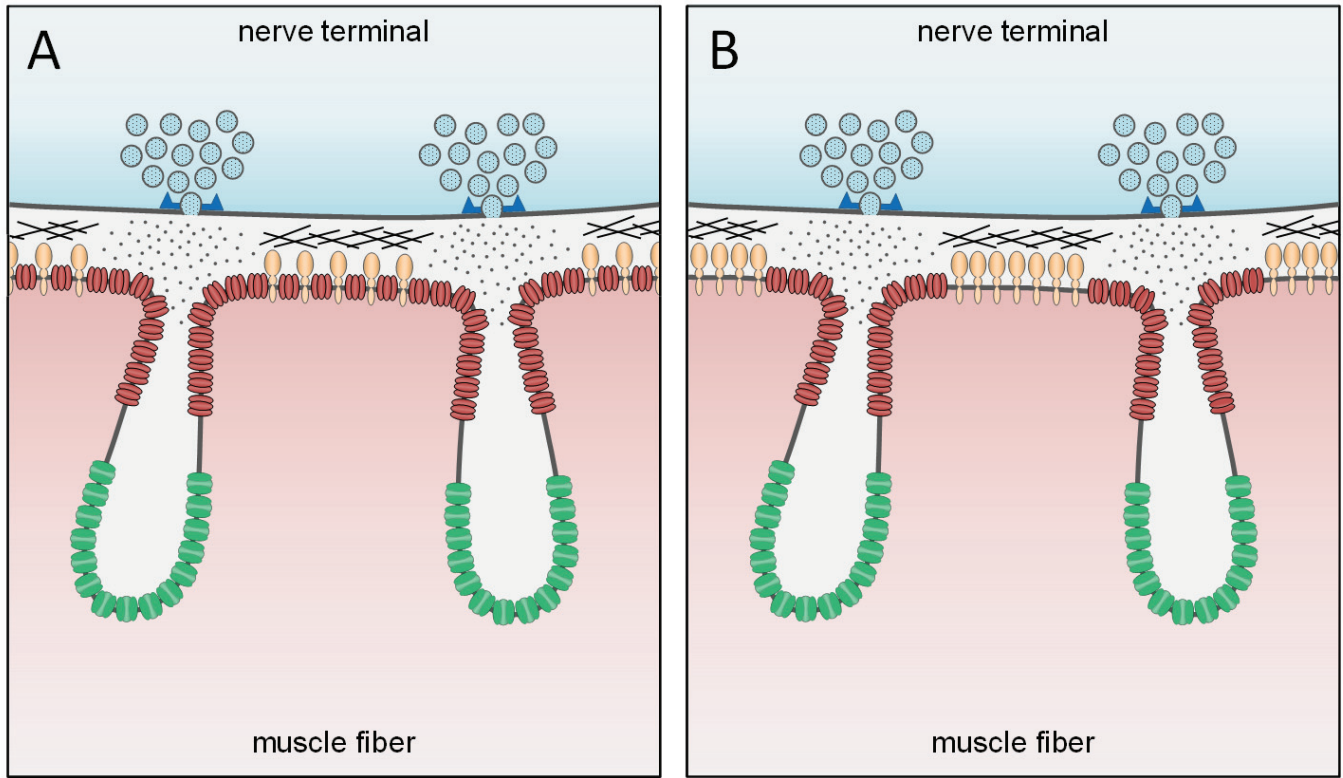
B



C







 AChR     Integrin  $\alpha7\beta1$      VGSC     AZ